Pergamon

Chaos, Solitons & Fractals Vol. 5, No. 11, pp. 2095–2107, 1995
Elsevier Science Ltd
Printed in Great Britain
0960–0779/95$9.50 + 0.00

0960–0779(95)00007-0

Multiparameter Model of a Dissipative Nonlinear Oscillator in the Form of One-Dimensional Map

B. P. BEZRUCHKO, M. D. PROKHOROV and E. P. SELEZNEV

Saratov Branch of the Institute of Radioengineering and Electronics, Russian Academy of Sciences, 38, Zelyonaya str., Saratov 410019, Russia

Abstract—A method is described for constructing directly from a time series a one-dimensional map which simulates the dynamics of dissipative nonlinear oscillator under pulse excitation. On the base of physical experiment, a procedure of determining the model parameters is proposed. The influence of selecting a dynamical variable on the model's dimension is demonstrated.

1. INTRODUCTION

Construction of dynamical model equations from a fluctuating time series is one of the most important problems in nonlinear science. In general case, this problem is very complicated. It is closely studied [1–3] but is not likely to achieve termination. However, in some cases using additional information and restricting the class of considered systems, one is able to facilitate substantially the model's construction, as well as to simplify the procedure of its parameters determination. For example, the effective dimension of the system is reduced if its dissipation is high enough within a characteristic time. The decrease of the model dimension can be sometimes achieved by successful selection of the dynamical variables and by passing from differential equations to maps. The low-dimensional model maps have already demonstrated their efficiency when describing transition to chaos. Particularly, the use of one-dimensional maps give an impressive advance towards revealing several types of universal behavior which are common for systems of different nature [4].

In the paper, the one-dimensional map model of a driven dissipative oscillator is constructed with the nonlinear pendulums, mechanical and electrical, ('modernized' clock pendulum and LR-diode circuit shown in Fig. 1). A great damping is introduced into the systems at the moment of periodic pulse excitation. The one-dimensional multimodal map (2) is obtained by suitably selecting the variable. The map involves four parameters which have a pronounced physical sense. The procedure of determining the parameters from experimental data is described. The arrangements of the model parameter space and of the experimental system (LR-diode circuit) are compared. The influence of selecting the dynamical variable on the model map's form is demonstrated when processing the time series.

2. SIMULATION OBJECTS

Consider a dissipative oscillator with the exponentially damping natural oscillations having the form:

$$x(t) = x_0 \mathrm{e}^{-\delta t} \cos\left(\frac{2\pi}{T_0(1 + \beta x_0)} t\right), \tag{1}$$

where x_0 is an initial deviation, T_0 is the oscillation period at $x_0 \to 0$, and the constants δ

and β define damping and nonlinearity, respectively. An essential feature of the systems simulated is the dependence of oscillation period on x_0.

Such a situation may be assumed for the mechanical clock's pendulum (Fig. 1a). Here, the period of the pendulum natural oscillations is varied proportionally to the initial deviation from the equilibrium point by means of a clamp C which controls the length of operating spring section (as it is made to speed up or to slow down the clock). If the pendulum is periodically pulse excited at $t = nT$ moments (n is an integer and T is the driving period) in such a way that it instantly stops, swings by an angle A with respect to the position, where it has been at the excitation moment, and is left free again, then the forced oscillations $x(t)$ should have the form indicated in Fig. 1b. The technical realization

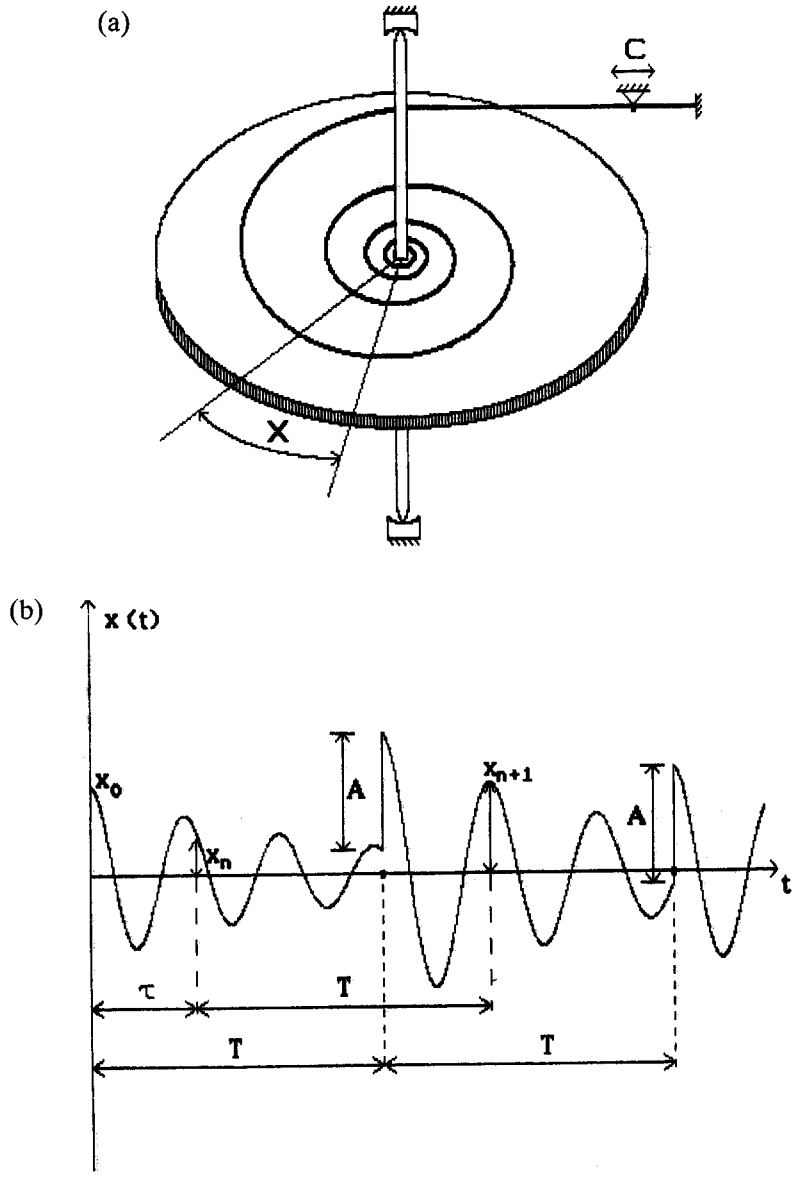

Fig. 1.(a) and (b).

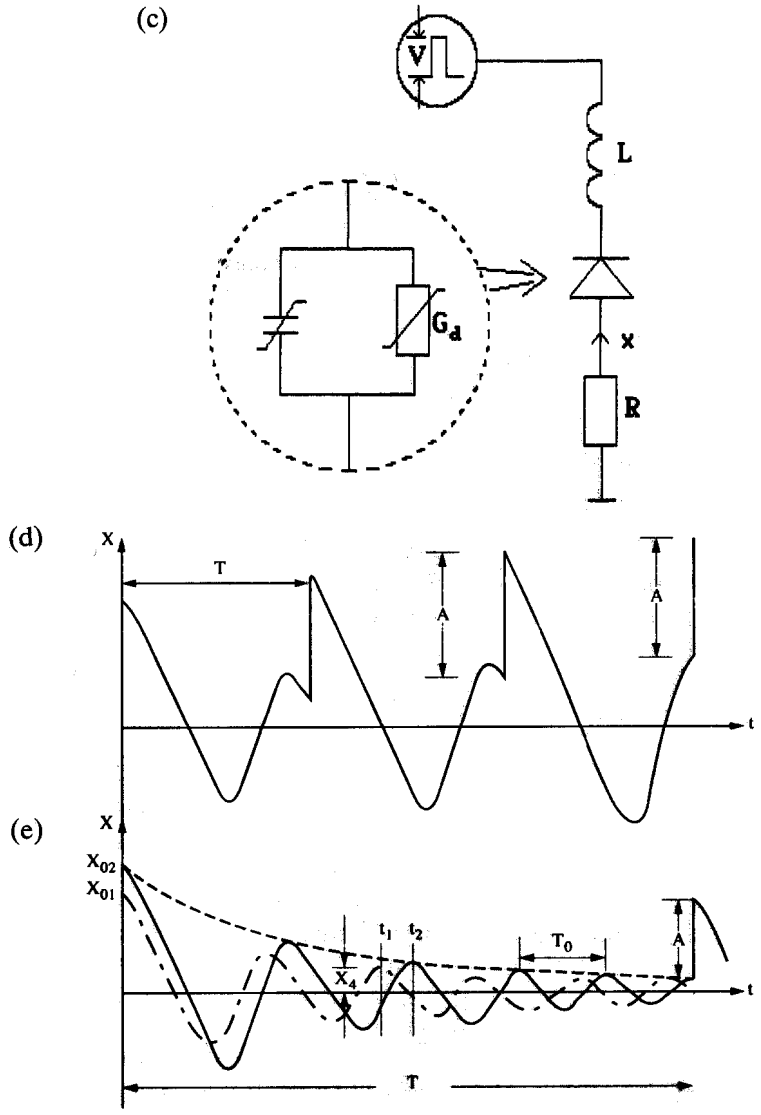

Fig. 1. (a) Mechanical pendulum with the operating restoring spring length varying by means of the clamp C. x is the angle of rotation about the equilibrium point; (b) Time dependences of the pendulum oscillations. The pendulum is excited by pulses at the moments marked by points on the axis. High damping is introduced at these moments. The rate of $x(t)$ variation is the same after the pulse excitation is terminated; (c) Electrical pendulum (LR-diode circuit) and the source of external emf. x is current in the circuit, V is the pulse amplitude. In a circle, a diode model is indicated consisting of nonlinear capacitance in parallel with nonlinear conductance. At forward currents, the equivalent active conductance of the diode G_d is high resulting in increased losses in the circuit; (d), (e) Time dependences of current oscillations in the LR-diode circuit under periodical excitation by short forward current pulses at various relations between the driving period T and the period of small natural oscillations T_0.

versions for the above example, that introduces great damping, are rather artificial for the clock pendulum.* As for the electrical pendulum, a diode resonator system (Fig. 1c), similar situation takes place when exciting current pulses have a forward polarity and minority carriers inject into the diode base. In this case, conductance in the equivalent diode circuit (see Fig. 1c) is high and thus, energy losses are sharply increased. A typical view of current oscillations in the considered driven circuit is shown in Fig. 1d and e for different values of driving period T. The initial oscillation phases are the same after termination of each pulse, just as in the mechanical example.

3. MODEL EQUATION AND ITS PROPERTIES

To construct a model return map, select the points spaced by the interval T on the fluctuating time series caused by external force (Fig. 1b), i.e., perform strobing, and establish a functional coupling between successive x_n values. The form of the return map depends on the strobing moment chosen. We will define this moment by the time interval τ starting after the exciting pulse is over (Fig. 1b). Note that τ variation means some change of variables. In the most simple case, as τ tends to zero, (1) gives the following one-dimensional multiparameter map:

$$x_{n+1} = A + x_n e^{-a/N} \cos\left(\frac{2\pi}{N(1 + \beta x_n)}\right), \tag{2}$$

where A is the driving amplitude, $N = T_0/T$ is the normalized driving frequency, $a = \delta T_0$ is the nonlinear damping, and β is the nonlinearity. Expression (2) can be renormalized to the three-parameter form:

$$z_{n+1} = 1 + A_1 z_n \cos\left(\frac{1}{A_2(1 + A_3 z_n)}\right), \tag{3}$$

where $z_n = x_n/A$, $A_1 = \exp(-a/N)$, $A_2 = N/2\pi$, $A_3 = \beta A$. In (3) all the parameters and the variable are dimensionless but the physical sense of the parameters is less clear. The previously reported results of investigation of the driven oscillator's dynamics, particularly, the results obtained for the nonlinear circuit [5–8] are traditionally represented for the variables and parameters close to the used in (2). With regard to the above mentioned, consider further just this model, assuming a conveniently selected units for x_n and β in Section 5 under comparison with the experiment.

The plot of the map (2) has a shape of a sinusoid, modulated in amplitude and frequency. It is bounded by two crossed straight lines sloping towards the horizontal axis by the angle $\alpha = \pm\text{arctg}\,(\exp(-a/N))$. The frequency is varying along the x_n axis in such a way that it tends to infinity at the point $x_n = -1/\beta$ and decreases, tending to zero, while moving from this point to the left and to the right (Fig. 2). The extrema of function $f(x_n)$ are placed at the points $x_n = (2/mN\beta) - (1/\beta)$, where m is a nonzero integer. The extrema that are most distant along the x_n axis correspond to $m = \pm 1$, i.e. they are at the points $x_n = (\pm 2 - N)/\beta N$. Parameter N defines the rate of frequency variation and β relates to the scale in the horizontal. The β increase results in the curve compression along the x_n axis. The vertical shift of the function plot is defined by the A value. In the region where

*This may be a flywheel with the mass far exceeding the mass of a pendulum which rotates with the rate of angular motion $2\pi/T$ about the axis being perpendicular to that of the pendulum. The situation described is realized under nonelastic interaction (e.g., if the flywheel having a convex friction sector with the angle A catches on the pendulum). The spring length is varied by a special lever. In the simplest case, one may stop and turn the pendulum with the hand.

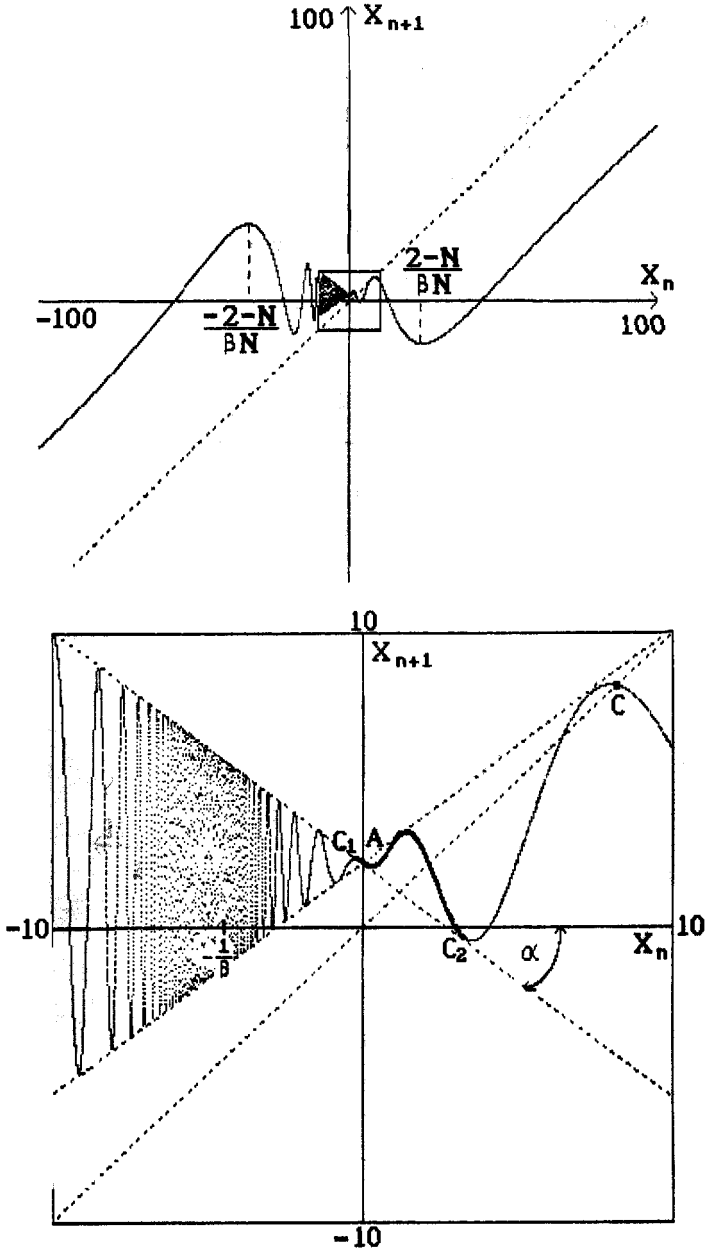

Fig. 2. The plot of the function (2) for the parameter values $A = 2.2$, $a = 0.1$, $N = 0.4$, $\beta = 0.2$. In the enlarged fragment the equilibrium point C and the points visited when moving on another attractor, the chaotic one (section C_1C_2), are marked.

$x_n > 0$, the plot of the map (2) is similar in shape to one obtained in [9] for a system with a triple instability.

Equation (2) can have periodic or chaotic solutions. At some parameter values, several solutions may exist, i.e., multistability can be observed when the system behavior is defined by the initial conditions. For example, Fig. 2 depicts a situation when there exist two attractors in phase space, the chaotic one and the equilibrium point.

4. ARRANGEMENT OF THE PARAMETER SPACE

In Figs 3 and 4, the parameter space structure of the system (2) is cited. The arrangement of the parameter space is easier to represent if one discerns some characteristic details. So, solid lines in Fig. 3a are the lines in the (N, A) plane where the multipliers of the driving period cycles (period-1 cycles) take the value of $+1$. These lines bound the regions which are represented at the sheets 0, I, II, III, ..., where various period-1 cycles exist and evolve to chaos. The region boundaries are the lines of folds converging at the cusp point at low and very high A values. If one constructs on the plane the lines of the highest multiplier values at $A \to 0$, they will connect the cusp point with the

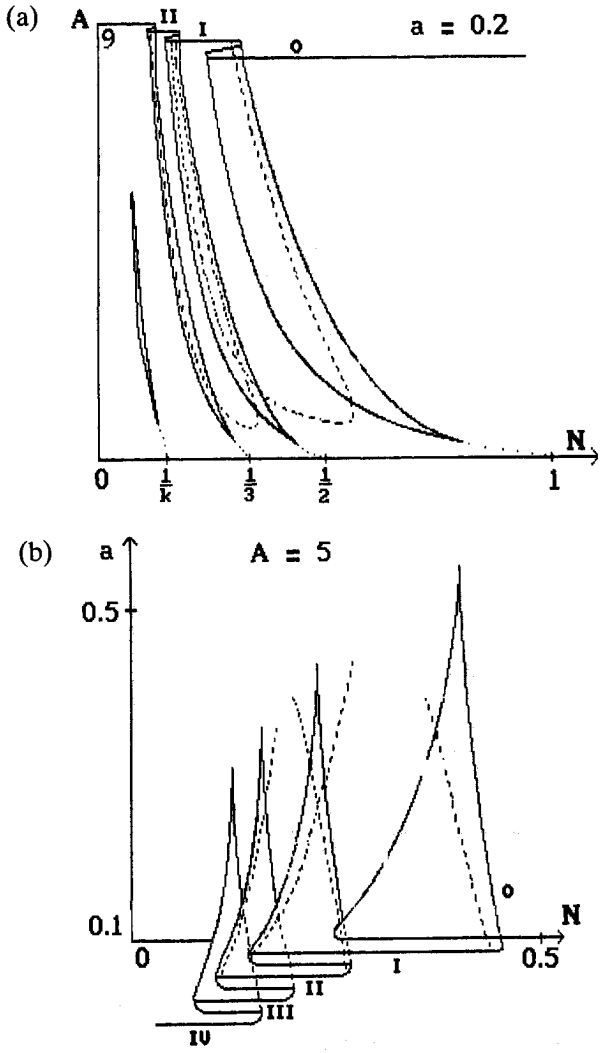

Fig. 3. The structure of the two-dimensional projections (N, A) and (N, a) of the model's (2) parameter space at $\beta = 0.2$. The regions of various period-1 cycles are represented in the sheets 0, I, II, ... The period doubling bifurcation lines are presented in the sheets I and II by dashed lines. The resonance lines are shown by dotted lines. With expanding the (N, A) plane (Fig. 3(a)) upwards, as A is increased, the lines are closed in pairs and the configurations of the upper regions are similar to the lower part of the figure. Below the value $a = 0.1$ (Fig. 3b), the parameter space structure is represented arbitrarily for visualization.

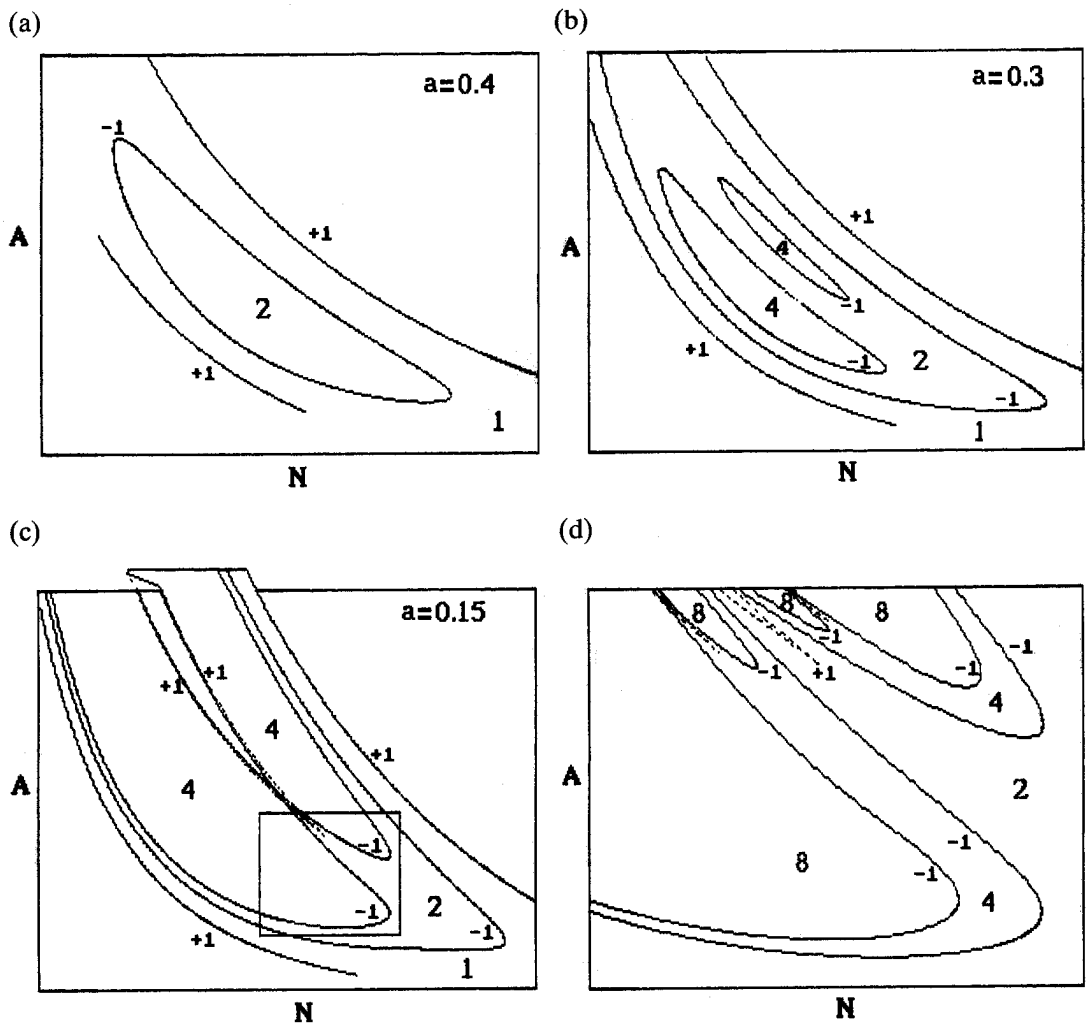

Fig. 4. Various oscillation regions of the model (2) in the driving parameter plane (N, A) for the sheet I as a function of the damping a. With numerals ± 1 the lines of multipliers of limit cycles which exist on the sheet I are denoted. Notations 1, 2, ... correspond to the periodic oscillation regions with the period being a multiple of the driving period T. The oscillation regions with periods exceeding 4 (except d) and chaotic regions are not presented. The fragment marked in b is enlarged in d. Scales: (a), (b) $N_{\min} = 0.15$, $N_{\max} = 0.55$, $A_{\min} = 0$, $A_{\max} = 12$; (c) $N_{\min} = 0.15$, $N_{\max} = 0.6$, $A_{\min} = 0$, $A_{\max} = 8$; (d) $N_{\min} = 0.35$, $N_{\max} = 0.48$, $A_{\min} = 1$, $A_{\max} = 3.5$.

axis N at the point $N = 1/k$, $k = 1, 2, 3, \ldots$. This corresponds to a main resonance and the resonance on subharmonics. At parameters corresponding to the sheets overlap, the multistability takes place. By moving over the plane above and below the multistability regions, one can pass from one cycle to another softly, with no hysteresis. The hysteresis occurs when crossing the above regions.

Dashed lines in Fig. 3a are the lines of multiplier -1 which correspond to period doubling bifurcation of period-1 cycles. These bifurcation lines bound the regions of complicated oscillations, and just that with a period exceeding the driving period and chaotic ones. For simplicity, they are presented for the sheets I and II only. Similar structure is obtained for the (N, a) plane in Fig. 3b. Together with Fig. 3a, it allows one to represent the arrangement of the considered regions in the space of three parameters

(N, a, A). It is seen from Fig. 3b that the complicated oscillation regions based on different period-1 cycles are separated in the space under high dissipation, but with decreasing damping a they intersect in the multistability regions. Near the cusp points a configuration is realized in the parameter space known as the crossroad area (Fig. 3a, b) [10].

Taking into account that different complicated oscillation regions are arranged identically, consider in more detail only the sheet I at successively decreasing a values (Fig. 4). If only period-2 cycle exists under high dissipation within the discussed intervals of parameters A and N in the complicated oscillation region (Fig. 4a), then, with decreased damping, two nonoverlapping period-4 cycles are revealed inside the region (Fig. 4b). At smaller dissipation values the multistability appears inside the region I and the crossroad area is again realized in the section (Fig. 4c). It is interesting to note that, as damping decreases, the lower "beaks" of the period-2 regions tend to $N = 2/(2k + 1)$ where $k = 1, 2, 3, \ldots$. Thus, the chosen complicated oscillation regions turn out to be filled by typical structures which are similar to that presented in Fig. 3. As a result, at arbitrary motion over the parameter space a transition to chaos can be observed via a sequence of period doubling bifurcations or via different hard transitions that one is able to imagine while looking at Fig. 5. In the chaotic regions there exist wide windows of period-3 cycles which also evolve to chaos via the sequence of period doubling bifurcations and maintain the above features.

The structure of the parameter plane (N, β) is similar to that considered for the (N, A) plane. Figure 6 demonstrates the influence of parameter β on the shape of the complicated oscillation regions. As β increases with the other parameters fixed, the complicated oscillation regions in the (N, A) plane deviate stronger from the vertical. As β and A vary such that $\beta A = \text{const}$, the form of oscillation is not changed.

5. DETERMINATION OF THE MODEL'S PARAMETERS FROM EXPERIMENT. COMPARISON OF EXPERIMENTAL AND NUMERICAL RESULTS

Using the maps (2) and (3) as a model of the diode circuit (Fig. 1(c)), we determined the parameter values from the time dependences of current in the circuit driven by short (compared to T_0 and T) pulses from the current source. An oscillogram shown in Fig. 1(d), corresponds to the case when T is insignificantly higher than T_0. As T increases the natural oscillation period shows dependence on the amplitude (the pendulum's nonisochronism (Fig. 1(e)).

The parameters of the model can be determined by the current oscillogram (Fig. 1(e)) in the following way:

- $N = T_0/T$, where T_0 is the period of small amplitude oscillations, and T is the driving period;
- a is determined from the exponential approximation of an envelope denoted in the figure by a dashed line;
- A is determined by the current jump in the circuit at the moment of pulse excitation;
- β is determined by using the ratio:

$$\beta = \frac{t_2 - t_1}{t_1 x_{02} - t_2 x_{01}}, \tag{4}$$

where t_1 and t_2 are the moments of time which correspond to a certain fixed oscillation phase value, for example, to the function $x(t)$ extremum as it is shown in Fig. 1e. These moments are taken for different initial amplitudes x_{01} and x_{02} measured by the same

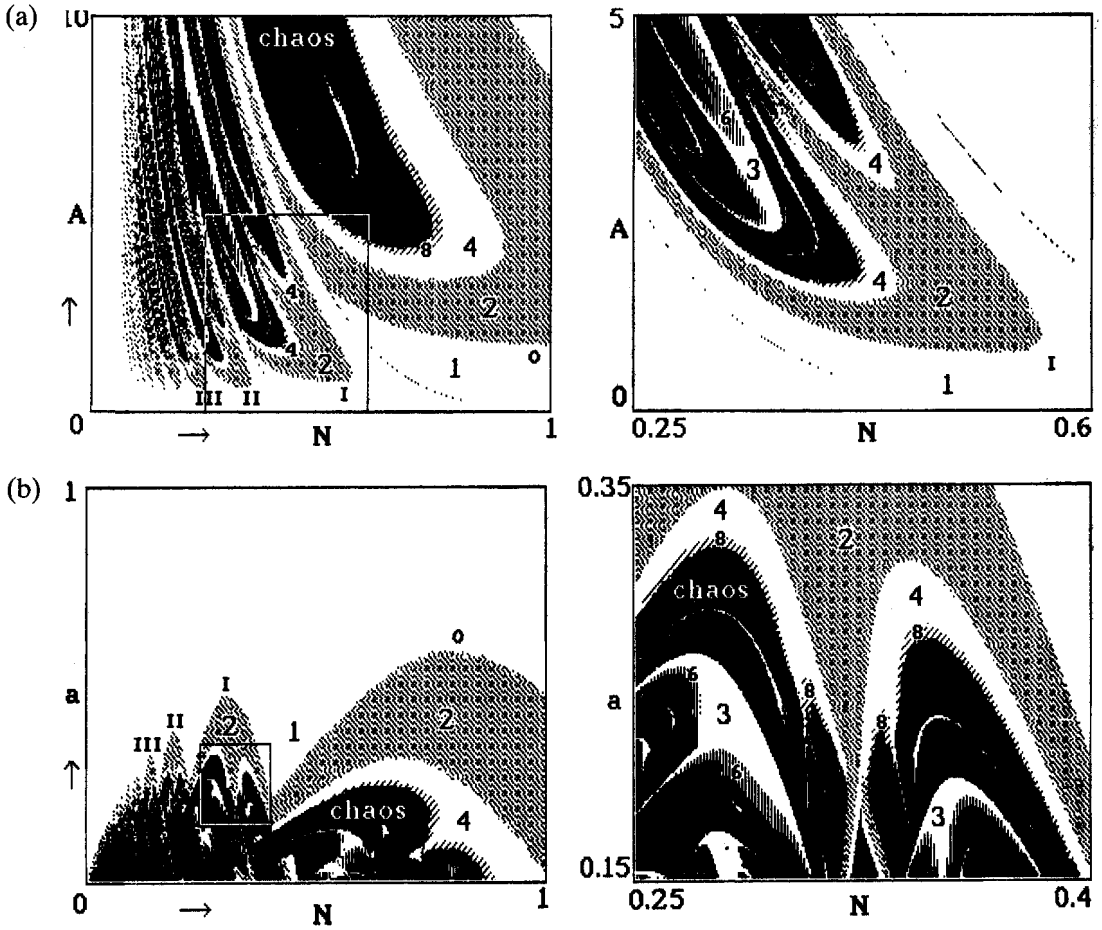

Fig. 5. The structure of the model (2) parameter space obtained by one-directionally moving in the direction shown by arrows near the axes. In the enlarged fragment of a only the structure of the sheet I is shown. Notations 1, 2, 3, ... correspond to the periodic oscillation regions with periods being a multiple of the driving period T. The chaotic oscillation regions are painted in black color and labeled as 'chaos'.

units as A. The β value thus obtained for the nonisochronous pendulum depends on the magnitudes of $t_{1,2}/T_0$. It is expedient to choose the t_1 and t_2 values such that the number of oscillations on these time intervals was close to $1/N$ in the model equation.

There are other methods to experimentally determine the parameters. So, N can be determined as the driving frequency-to-linear resonant frequency ratio. One is able to find a by measuring the circuit's Q factor at a low driving amplitude with respect to the known relationship between damping decrement and Q factor: $a = Q/\pi$. The nonlinearity parameter can be found with the help of the following relation:

$$\beta = \frac{1}{x_0} \times \left\{ \frac{2\pi t_1}{T_0[\arccos(x_1/x_0 \times \exp(at_1/T_0)) + 2\pi k]} - 1 \right\}, \tag{5}$$

where k is an integer, the number of oscillations $x(t)$ for the time t_1 (Fig. 1e, $k = 2$).

The β dimension and absolute value is defined by choosing the units of measurement for A and x_0. But the choosing does not affect the qualitative form of the parameter space

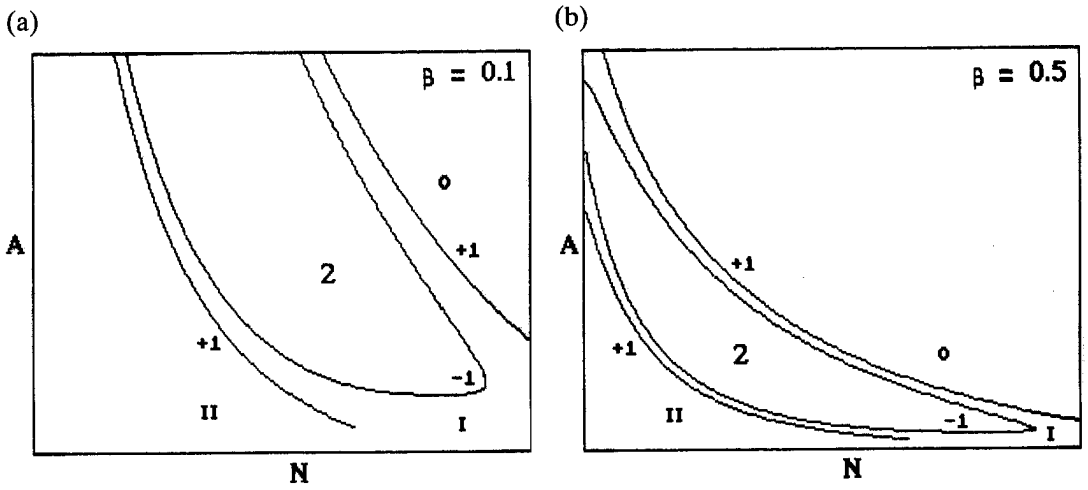

Fig. 6. Deformation of the sheet I structure of the (N, A) plane with varying the parameter β, $a = 0.2$. Oscillation regions with period exceeding 2 and chaotic ones are not presented. Scales: $N_{min} = 0.1$, $N_{max} = 0.6$, $A_{min} = 0$, $A_{max} = 12$.

structure. For example, with the 5-fold scale decrease in A, the lines in Fig. 6(b) will coincide with the lines in Fig. 6(a) where the β value is 5 times smaller.

For a particular LR-diode circuit, we have experimentally constructed the driving parameter plane where the regions of existence and evolution of various driving period cycles are illustrated (Fig. 7a). The scale in A and x was established to agree with the scale in Fig. 3a which was constructed under numerical investigation of (2). The bifurcation line configurations in both the figures are similar. Then, the bifurcation lines were experimentally constructed for the sheet I, Fig. 7b. According to the approach proposed, we determined the β value at the number of oscillations equal to 2 within the observation interval t_1. It corresponds best of all to N close to 1/2, and it turned out to be about 0.2. Other parameters were found too. In the end, the data of physical experiment and that of numerical model investigation were compared at close parameters. Comparing the arrangement of the (N, A) planes at fixed a and β values, (see Fig. 7 and Figs 3(a), 5(a)) one may conclude about a good enough agreement between the model and the object behaviors in the region $N < 1$. The shapes and location of the same period cycles are close. The positions of some hard transition lines coincide, as well as some other details agree.

However, the model does not represent the features of the experimental system at $N > 1$. In the real system, at $1 < N < 2$, a sequence of period adding cycles exist. These cycles evolve to chaos similarly to the harmonic driving case [5, 6, 7, 8, 11]. As for the model, the complicated oscillation regions are actually absent within this interval of N values. The region marked in Figs 3, 4 and 5 by 0 is the last one and its configuration differs sharply from its experimental shape.

6. DEPENDENCE OF THE MODEL PROPERTIES ON CHOOSING A DYNAMICAL VARIABLE

Consider the influence of τ choosing on the form and properties of the model map. For an arbitrary τ, the return map can be written using eq. (1) only in the nonexplicit form:

$$y_{n+1} = f(y_n, x_n) = f(y_n, g(y_n)), \tag{6}$$

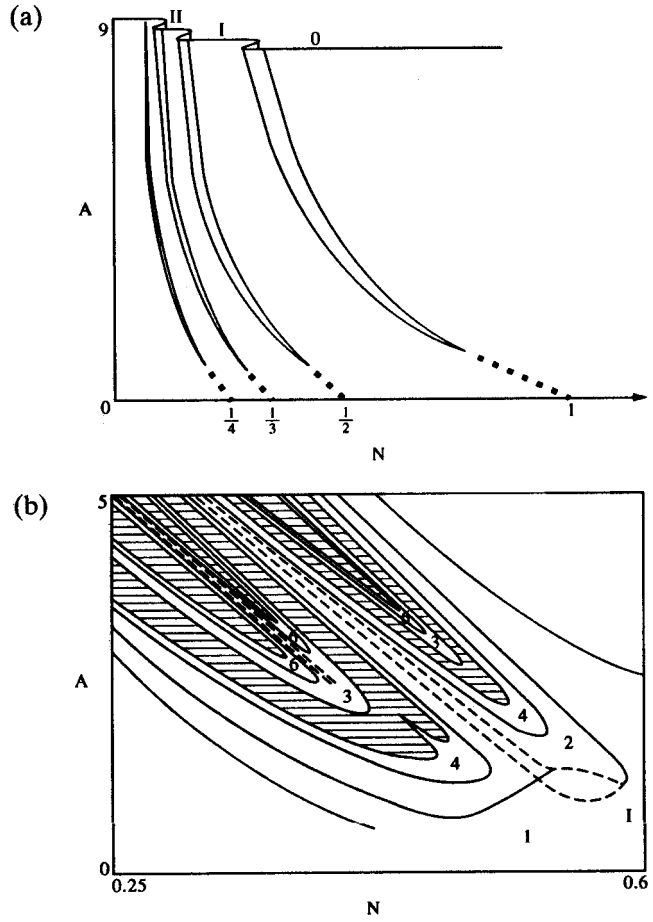

Fig.7. The structure of the driving parameter plane of the LR-diode circuit. The regions of various period-1 cycles (a) and arrangement of these regions with indicated oscillation periods (b). Hatched are the regions of chaotic oscillations. The hard transition lines are shown by dashed lines.

where

$$y_n = x_n e^{-\delta\tau} \cos\left(\frac{2\pi}{T_0(1 + \beta x_n)}\tau\right)$$
$$y_{n+1} = x_{n+1} e^{-\delta\tau} \cos\left(\frac{2\pi}{T_0(1 + \beta x_{n+1})}\tau\right). \quad (7)$$

Numerical experiment enables one to analyze the map shape for various fixed τ values (see fragments in Fig. 8) and to compare it with that shown in Fig. 2. In general case, the map is not one-to-one, i.e., several x_{n+1} values correspond to one x_n value. Discrepancy between the values of x_{n+1} decreases with the increase of the damping δ. It is remarkable that, in spite of substantial model map differences and attractor differences due to selection of the dynamical variable, a complete agreement is observed between the structure of the map (6) parameter space and the structure shown in Figs 3–5 for the map (2). That is, that the system's dynamics is unambiguously defined by the observed time series. The variable selection can depend on convenience and goal of simulation.

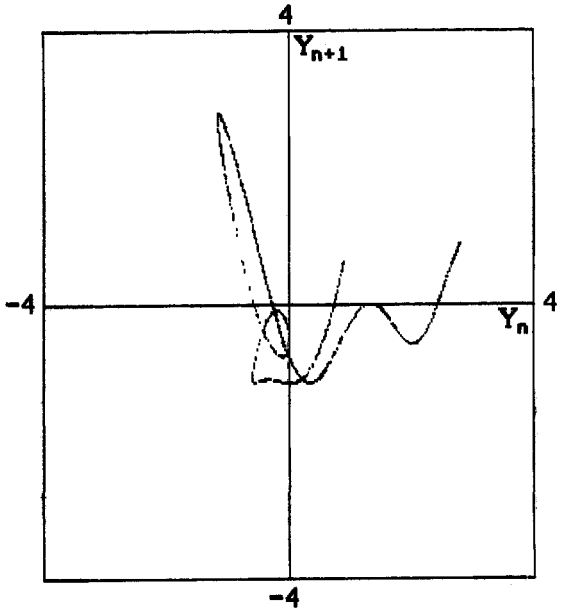

Fig. 8. The plot of y_{n+1} vs y_n obtained with respect to equation (7) at the point movement on the chaotic attractor, $\tau = 1.8$, $\delta = 0.01$, $\beta = 0.2$, $T_0 = 1$, $T = 2.5$, $A = 2$.

7. CONCLUSION

Thus, we have proposed and investigated the one-dimensional multiparameter model of the dissipative nonlinear oscillator with the parameters defined from the physical experiment's data. The model describes the behavior of the real system, the LR-diode circuit driven by current pulses at driving frequencies below the linear resonant frequency. It makes it possible to discern the feasible oscillations including the chaotic ones and to predict the arrangement of the system's parameter space structure without writing and solving differential equations. It is of interest that in the parameter region $N < 1$, the model represents the parameter space structure for the circuit driven by harmonic force [12–14]. It demonstrates also several features and the parameter space configurations typical for oscillators with nonsymmetric potential [15]. All the above is an evidence for the approach proposed to be promising for simulating highly dissipative systems.

Acknowledgements—We thank D. I. Trubetskov, S. P. Kuznetsov, A. P. Kuznetsov, and I. R. Sataev for helpful discussion of the paper and expert opinions. This work was supported by the Russian Foundation of Fundamental Research, grant No 93-02-16171.

REFERENCES

1. M. Casdagli, Nonlinear prediction of chaotic time series, *Physica D* **35**, 335–356 (1989).
2. G. Gouesbet and J. Maquet, Construction of phenomenological models from numerical scalar time series, *Physica D* **58**, 202–215 (1992).
3. G. Rowlands and J. C. Sprott, Extraction of dynamical equations from chaotic data, *Physica D* **58**, 251–259 (1992).
4. A. P. Kuznetsov and S. P. Kuznetsov, Critical dynamics of coupled map lattices at the onset of chaos, *Izv. VUZOV Radiophysics* **34**(10–12), 1079–1115 (1991).
5. H. Ikezi, J. S. de Grassie and T. H. Jensen, Observation of multiple-valued attractors and crises in a driven nonlinear circuit, *Phys. Rev. A* **28**(2), 1207–1209 (1983).
6. S. Tanaka, T. Matsumoto and L. O. Chua, Bifurcation scenario in a driven R-L-diode circuit, *Physica D* **28**, 317–344 (1987).

7. Z. Su, R. W. Rollings and E. R. Hunt, Simulation and characterization of strange attractors in driven diode resonator systems, *Phys. Rev. A* **40**(5), 2698–2705 (1989).
8. A. A. Kipchatov, Features of the complicated dynamics of the driven nonlinear oscillator, *Izv. VUZOV Radiophysics* **33**(2), 182–190 (1990).
9. A. Arneodo, P. H. Coullet, E. A. Spiegel and C. Tresser, Asymptotic Chaos, *Physica D* **14**, 327–347 (1985).
10. J. Carcasses, C. Mira, M. Bosch, C. Simo and J. C. Tatjer, Crossroad area – spring area transition (I) Parameter plane representation, *Int. J. Bifurcation and Chaos* **1**(1), 183–196 (1991).
11. J. Testa, J. Perez and C. Jeffries, Evidence for universal behavior of a driven nonlinear oscillator, *Phys. Rev. Lett.* **48**(11), 714–717 (1982).
12. J. Baxter, M. Bocko and D. Douglass, Behavior of a nonlinear resonator driven at subharmonic frequencies, *Phys. Rev. A* **41**(2), 619–625 (1990).
13. T. Klinker, W. Meyer-Ilse and W. Lauterborn, Period doubling and chaotic behavior in driven Toda oscillator, *Phys. Lett.* **101A**(8), 371–375 (1984).
14. V. V. Astakhov, B. P. Bezruchko, E. P. Seleznev, Variation of the parameter space structure of a stochastic system under additional mode excitation, *Pisma v ZhTF*, **13**(8), 449– 452 (1987).
15. C. Scheffczyk, U. Parlitz, T. Kurz, W. Knop and W. Lauterborn, Comparison of bifurcation structures of driven nonlinear oscillators, *Phys. Rev. A* **43**(12), 6495–6502 (1991).